International Journal of Nanoelectronics and Materials
IJNeaM
ISSN 198-5761 | E-ISSN 2232-1535

Advancing COVID-19 Detection: High-Performance RNA Biosensing via Electrical Interactions

Uda Hashim[a,b], M. N. Afnan Uda[b,*], M. N. A. Uda[a,c,d], Tijjani Adam[e], Nur Hulwani Ibrahim[a], Chai Chang Yii[b] and Lorita Angeline[b]

[a]*Institute of Nano Electronic Engineering, Universiti Malaysia Perlis, 01000 Kangar, Perlis, Malaysia.*
[b]*Faculty of Engineering, Universiti Malaysia Sabah, 88400 Kota Kinabalu, Sabah, Malaysia.*
[c]*Faculty of Mechanical Engineering & Technology, Universiti Malaysia Perlis, 02600 Arau, Perlis, Malaysia.*
[d]*Centre of Excellence for Biomass Utilization, Universiti Malaysia Perlis, 02600 Arau, Perlis, Malaysia.*
[e]*Faculty of Electronic Engineering & Technology, Universiti Malaysia Perlis, Kampus Tetap Pauh Putra, 02600, Arau, Perlis, Malaysia.*
**Corresponding author. Tel.: +60-194728844; e-mail: nurafnan@ums.edu.my*

ABSTRACT

This research paper investigated the detection of COVID-19 using an Aluminum Interdigitated Electrode (Al-IDE) sensor based on electrical conductivity. The silanization process involved the functionalization step, employing (3-Aminopropyl) triethoxysilane (APTES), while the immobilization process was facilitated by the RNA Probe specific to COVID-19. To verify its specificity in detection, the functionalized biosensor was tested against single-base mismatches, non-complementary sequences, and complementary sequences. The physical characteristics of the Al-IDE biosensor were examined using both low-power microscopy (LPM) and high-power microscopy (HPM). Additionally, the morphological properties of the biosensor were assessed using atomic force microscopy (AFM). To assess its diagnostic potential, the biosensor's sensitivity was evaluated by exposing it to a range of complementary targets, spanning from 1 femtomolar (fM) to 1 micromolar (µM). The current-voltage (I-V) characteristics of the biosensor were meticulously analyzed at each stage of functionalization bare Al-IDE, silanization, immobilization, and hybridization. This I-V characterization was carried out using a picoammeter voltage source (Keithley 2450), Kickstart software, and a probe station. The results confirmed the biosensor's capability to effectively detect COVID-19 targets within the nanoampere concentration range, demonstrating its success in detecting specific COVID-19 targets at the nanoampere level.

Keywords: *Aluminium Interdigitated Electrode, Biosensor, RNA COVID-19, Selective, Sensitive*

1. INTRODUCTION

The COVID-19 pandemic, which began in 2019, has developed into an unparalleled worldwide crisis, demanding creative solutions to control its transmission and consequences. A fundamental aspect of managing this pandemic effectively revolves around having strong and swift diagnostic tools [1], [2]. Nevertheless, their drawbacks related to accessibility, speed, and sensitivity have emphasized the pressing requirement for alternative diagnostic approaches [3]. As a response to these challenges, researchers have undertaken a mission to create advanced diagnostic technologies that combine affordability, portability, rapid detection, and ease of use, making them suitable for widespread adoption within healthcare systems [3], [4]. This effort aligns with the changing landscape of medical research, where fields like biotechnology and electronics are converging to develop state-of-the-art solutions [5], [6]. Consequently, a new approach has emerged electrical-based biosensors for detecting COVID-19 [7]–[9].

The ongoing COVID-19 pandemic has underscored the urgent need for rapid and accurate diagnostic methods to mitigate the spread of the virus [10]–[12]. Among various detection techniques, electrical-based biosensors have emerged as promising tools due to their sensitivity, specificity, and potential for rapid detection [13]–[15]. Previous studies in this field have made significant strides in developing biosensors for COVID-19 detection, showcasing their potential for clinical application [16]–[18]. However, despite these advancements, several limitations persist, including issues related to sensitivity, scalability, and cost-effectiveness [19], [20]. Therefore, there is a pressing need to address these drawbacks and further enhance the performance and practical utility of electrical-based biosensors for COVID-19 detection [21]–[23].

In this paper, we explore the detection of COVID-19 using the electrical conductivity of an Aluminum Interdigitated Electrode (Al-IDE) sensor. The main objective is to create a highly efficient biosensing platform capable of swiftly and accurately detecting the virus [24]–[26]. This pursuit gains significant importance in a pandemic, where timely and precise diagnosis is critical in implementing effective containment strategies and safeguarding public health.

The development of this biosensing platform involves a multi-step process. Initially, the Al-IDE sensor is functionalized through a silanization process utilizing (3-Aminopropyl) triethoxysilane (APTES). This step enhances the surface properties of the sensor, preparing it for subsequent stages [27]–[29]. Next, the sensor undergoes

immobilization, where RNA Probe COVID-19 is employed to create a specialized binding environment for the target RNA sequences related to the virus. An important aspect of this research is the exploration of the sensor's ability to differentiate between various RNA sequences. The functionalized biosensor is exposed to hybridization with different RNA sequences, including those with single-base mismatches, non-complementary sequences, and entirely complementary sequences. The successful discrimination of specific sequences highlights the sensor's potential for precise detection of COVID-19 [30]–[32]. This study highlights the significance of RNA biosensing by demonstrating its potential to enhance the early detection, monitoring, and management of infectious diseases, with a particular focus on COVID-19. This technology is pivotal in addressing current and future global health challenges. In RNA biosensing, specific molecular probes are designed to complement and bind to the target RNA sequences. These probes are often single-stranded DNA or RNA molecules with a known sequence that matches the viral RNA [33]–[35].

To comprehensively analyze the physical and morphological characteristics of the biosensor, microscopy techniques are employed. Low-power microscopy (LPM) and high-power microscopy (HPM) provide insights into the sensor's physical properties, while atomic force microscopy (AFM) offers a detailed view of its structural morphology. Additionally, the biosensor's sensitivity is assessed by exposing it to varying concentrations of complementary single-stranded DNA (ssDNA) targets, ranging from 1 femtomolar (fM) to 1 micromolar (μM). This evaluation provides valuable information about the biosensor's performance detecting a wide range of target concentrations.

Essential to the biosensor's operation is its current-voltage (I-V) characteristic, which undergoes scrutiny at various functionalization stages. These stages encompass the initial bare Al-IDE configuration, followed by silanization, immobilization, and finally, hybridization. The I-V characterization uses a picoammeter voltage source (Keithley 2450), Kickstart software, and a probe station, enabling a comprehensive understanding of the sensor's electrical behaviour. The culmination of this research confirms the successful detection capabilities of the Al-IDE biosensor. It demonstrates the sensor's ability to detect specific RNA targets associated with COVID-19 within the nanoampere concentration range.

2. MATERIAL AND METHODS

2.1. Chemical, Reagents and Instrument

The materials utilized in this study included Ethanol (C_2H_5OH) and (3-Aminopropyl) triethoxysilane (APTES) ($C_9H_{23}NO_3Si$), both of which met the criteria for analytical reagent grade and were obtained from commercial suppliers. The configuration of the Al-IDE mask was meticulously designed using AutoCAD Software, with the specific goal of creating a system for detecting COVID-19 RNA. After this detailed design process, the blueprint was transformed into a practical form using a commercial chrome mask sourced from Silterra (M) Sdn Bhd. This process ultimately led to the fabrication of the Al-IDE.

The characterization of the bare Al-IDE was systematically conducted through the application of various microscopy techniques. This involved the use of Low-Power Microscopy (LPM), High-Power Microscopy (HPM), and Atomic Force Microscopy (AFM), all employed together to determine the physical and morphological properties of the Al-IDE. Finally, the last phase of this comprehensive process involved conducting current-voltage (I-V) characterization measurements. To accomplish this, the (Keithley 2450) instrument, in conjunction with Kickstart software, was utilized to facilitate these assessments. The experimental setup was carefully arranged within a Probe Station, allowing for precise and controlled measurement procedures. Through this meticulous orchestration of processes and measurement methods, the research not only gained deeper insights into the physical and morphological characteristics of the Al-IDE but also derived invaluable I-V characteristics, enhancing understanding of its electrical properties with COVID-19 RNA detection.

2.2. Al-IDE Surface Functionalization

The Al-IDE electrode underwent a thorough cleansing procedure using ethanol, followed by a 5-minute drying period. Afterwards, the electrode was functionalized with the APTES compound through a meticulous silanization process. A precisely measured 2 μl of APTES was carefully dispensed onto the active region of the Al-IDE, resulting in the formation of a crucial 'active' layer that enhanced the electrode's functionality. This newly functionalized electrode was left to air dry at room temperature, specifically at 27°C, within a controlled environment dry cabinet for a duration of 30 minutes. Following this, a comprehensive PBS washing step was carried out, meticulously removing any unbound APTES molecules from the surface. An additional 5-minute drying cycle was then performed within the dry cabinet. The primary objective of this silanization process was to effectively coat the active surface area of the Al-IDE with organofunctional alkoxysilane molecules. In this context, APTES, widely recognized for its frequent application in silanization processes, was chosen as the preferred agent for functionalizing surfaces with alkoxysilane molecules.

After the silanization process was completed, the next step involved the immobilization of a RNA probe onto the surface of the electrode. This action initiated the creation of a recognition layer through covalent amide bonding between the carboxyl group of the RNA probe and the surface. The assembled structure was then allowed to air dry within the dry cabinet for 1 hour. Following this, a precise rinse using PBS was carried out, effectively removing any unbound probe RNA on the surface. Once again, a 5-minute drying period within the dry cabinet followed, preparing the Al-IDE biosensor to detect a range of distinct targets.

The hybridization process involved binding single-stranded RNA molecules to their complementary target RNA sequences. Specifically, 1 µl of RNA targets ranging from 1 femtomolar (fM) to 1 micromolar (µM) concentration were carefully deposited onto the Al-IDE biosensor to allow them to hybridize with the immobilized RNA probes. This hybridization process was allowed to proceed for 1 hour for each concentration. Following the hybridization, the Al-IDE surface was rinsed with PBS to remove unbound RNA targets. The current-voltage (I-V) measurements were used to detect changes in the nanoampere range throughout the silanization, immobilization, and hybridization processes. An illustration of the sensing surface is shown in Figure 1.

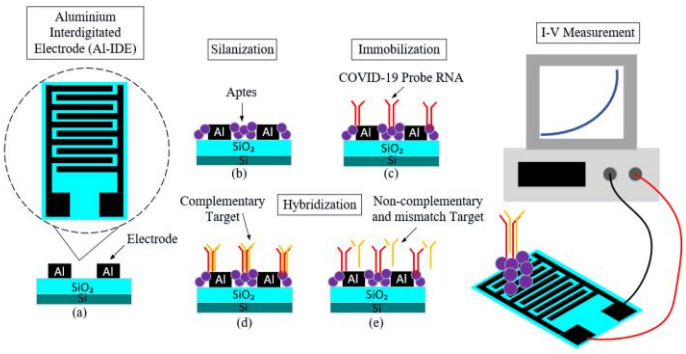

Figure 1. Illustration of Sensing surface (a) Bare Al-IDE (b) Al-IDE/APTES (c) Al-IDE/APTES/COVID-19 Probe RNA (d) Hybridization with COVID-19 complementary target (e) Hybridization with COVID-19 non-complementary and mismatch target.

3. RESULTS AND DISCUSSION

3.1. Surface Characterization

Figure 2 displays the physical characterization of the Aluminum Interdigitated Electrode (Al-IDE) using Low-Power Microscopy (LPM) and High-Power Microscopy (HPM). It is crucial to ensure the accurate fabrication of the Al-IDE to prevent any interference with measurements during the surface characterization process. These images were captured at different resolutions, specifically 5x, 20x, and 50x, providing essential details about the dimensions of the Al-IDE's finger width and the gap between the electrodes.

In the context of these images, Low-Power Microscopy (LPM) provides a clear visualization of the fabricated IDE structure, highlighting the complex configuration where the electrodes interconnect with the comb-like arrangement of finger electrodes, as emphasized in Figure 2(a). On the other hand, High-Power Microscopy (HPM) shifts the focus to a broader surface area, offering a comprehensive view free from contaminants or significant deviations from the desired structural integrity, as depicted in Figure 2(b).

The detailed depth provided by the 50x resolution images, as shown in Figures 2(c) and 2(d), delves into the subtle intricacies of the surface. It focuses explicitly on the Al-IDE functionalization process, which involves the addition of 2 µl of (3-Aminopropyl) triethoxysilane (APTES) at a concentration of 10 µM onto the active area of the Al-IDE. This crucial step in the silanization process aims to coat the Al-IDE's active region with a monolayer of APTES molecules. The resulting images not only confirm the careful execution of the functionalization process but also provide insights into the distribution and arrangement of the APTES molecules across the electrode surface.

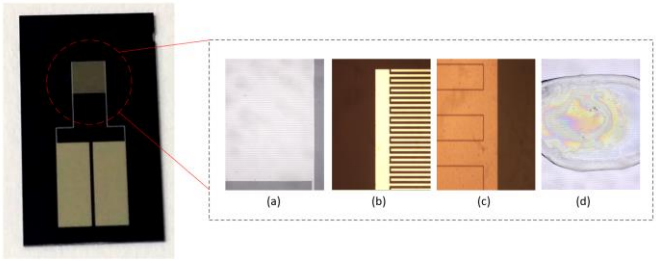

Figure 2. Al-IDE physical characterization using LPM and HPM images (a) 5x resolution, (b) 20x resolution, (c) 50x resolution and (d) after 2 µl APTES with 10 µM concentration.

The precise use of photolithography, a highly accurate technique known for its precision, plays a crucial role in transferring the complex IDE pattern onto the substrate surface. This technique enables a seamless alignment between the intended design and the actual structure, serving as a fundamental element that supports further exploration of the detailed electrical characteristics of the Al-IDE biosensor.

Central to the investigation, the Al-IDE's current-voltage (I-V) characteristics are dissected precisely. This quantitative exploration delves into the amplitude of electrical current coursing through the Al-IDE, unravelling the intricate dance of charge carriers within the complex architecture. The Al-IDE's geometric symmetry, with a finger width of 50 µm and inter-finger gap of 1 µm, assumes prominence in this analysis.

Figure 3 brings the Al-IDE's morphology to the fore through Atomic Force Microscopy (AFM). This topographic perspective meticulously unveils the IDE finger surface, accentuating its impeccable fabrication and the controlled 1 µm inter-finger gap. Notably, the AFM profiler spectrum underscores an Al layer thickness of approximately 20 nm, encapsulating the meticulousness intrinsic to the fabrication process. In unity, these analytical threads weave a comprehensive understanding of the Al-IDE's electrical and structural attributes, forming a vital nexus at the intersection of interdisciplinary scientific exploration. The I-V characterization was performed using (Keithley 2450), probe station and Kickstart software with Al-IDE biosensor to get I-V characteristics, as shown in Figure 4.

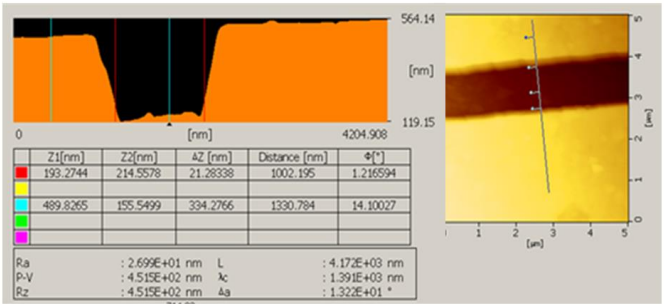

Figure 3. Al-IDE morphological characterization using AFM.

3.2. Electrical Characterization: Validation of Fabricated Al-IDEs

Before undergoing APTES functionalization, the bare Al-IDE underwent characterization for its current-voltage (I-V) properties using a Probe Station (Keithley 2450) in conjunction with Kickstart software, as illustrated in Figure 4. During the I-V characterization process, a voltage source ranging from 0 to 1 V was applied, with a precaution that exceeding this designated voltage threshold could potentially damage the Al-IDE sensor. The results were meticulously recorded and subsequently compiled using the Kickstart program in Microsoft Excel.

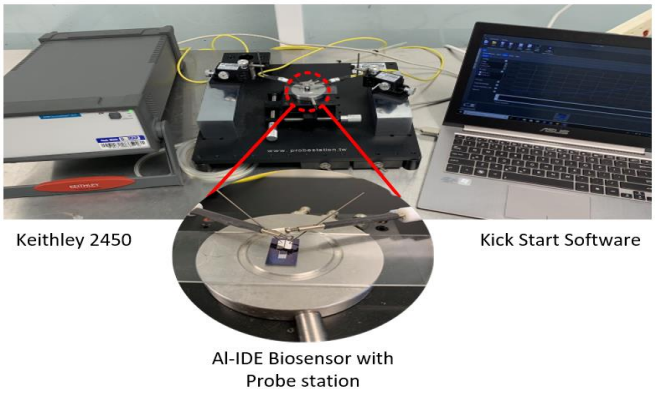

Figure 4. Electrical Characterization.

Before proceeding with the analysis of target single-stranded RNA samples, it was essential to conduct a thorough assessment of repeatability and stability for the Al-IDE biosensor. This critical phase of electrical characterization involved using five distinct Al-IDE instruments. Figure 5a, shows the discernible I-V properties of various bare Al-IDEs. Across the voltage spectrum, remarkable consistency in results is observed, with the latest iterations registering at 24.4 pA, 24.5 pA, 24.3 pA, 24.2 pA, and 24.0 pA, respectively, for each distinct bare Al-IDE. The well-defined benchmarks of typical low and high currents were established at 0.5 pA and 23.3 pA, respectively. These subtle variations highlight the precision in the fabrication and processing of the Al-IDEs.

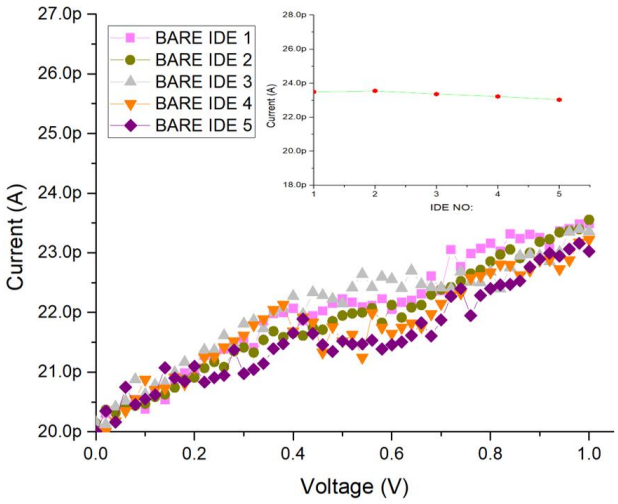

Figure 5. I-V Characteristics of Bare Al-IDE.

3.3. Chemical Functionalization: Chemical Assembly

Experiments were conducted to confirm the expected relationship between the current in the Aluminium Interdigitated Electrode (Al-IDE) and the quantity of chemical compounds on the substrate of the sensor. In essence, a higher current flow through the Al-IDE is correlated with an increase in the concentration of chemical substances. This pattern indicates that more chemicals or molecules are present in higher abundance, which helps more ions move through the Al-IDE structure. The current-voltage characteristics of the Al-IDE after chemical functionalization with COVID-19 probe RNA and APTES (3-aminopropyltriethoxysilane) are shown in Figure 6. Effective binding with the COVID-19 probe RNA is made possible by the functionalization process's integration of APTES, which is essential for creating contact between organic and inorganic surfaces. APTES is distinguished by the presence of a positively charged amine group, which is essential for improving the sensitivity and specificity of the sensor. In order to act as a sensing buffer during the silanization process, the concentration of APTES on the Al-IDE's active surface and in the space between the two electrodes was purposefully lowered. The current rose to 1.3 nA as the concentration of APTES dropped, demonstrating the direct relationship between chemical compound density and current flow through the Al-IDE. The sensor illustrates how SiO2 is converted into SiOH by the interaction of SiO2 surfaces with hydroxide ions (OH^-). This change modifies resistivity, which has a substantial impact on resistance. when a result, the region and distance between the Al-IDE's interdigitated electrodes stayed constant when the density of APTES on the surface decreased. Equation (2) illustrates how this occurrence increased the density of APTES because hydroxide ions (OH^-) were present, which improved conductivity. This wider current range was a result of the improved conductivity, which illustrates the complex interaction between surface characteristics, chemical functionalization, and electrical conductivity in the Al-IDE system.

The current increased to 1.3 nA as the APTES concentration during the silanization phase was reduced on the active area of the Al-IDE and between the two electrodes, effectively serving as a sensing buffer. When SiO_2 surfaces react with hydroxide ions, they transform into SiOH, as shown in Equation (1), and this transformation affects resistance by altering resistivity. As the density of APTES on the Al-IDE surface decreased, the distance and region between the interdigitated electrodes of the Al-IDE remained constant, leading to an increase in APTES density due to the presence of hydroxide ions (OH). This enhanced conductivity, as demonstrated in Equation (2), resulted in a broader current range.

$$\text{Resistivity, } R = \rho\iota/A \quad (1)$$

$$\text{Conductivity, } \sigma = \iota/\rho \quad (2)$$

With COVID-19 RNA samples serving as bio-receptors for the specific capture of COVID-19 RNA, 2 µl of COVID-19 probe RNA at a concentration of 10 M was immobilized on top of the APTES layer. The current recorded at 1 V for the COVID-19 probe RNA, as indicated by the curve in Figure 6, is 4.3 nA. Since RNA carries a negative charge, it results in an increased number of surface charges on the APTES layer. These accumulated positive charges continue to flow towards the negative side, leading to an elevation in the electric field. The higher current observed can be attributed to COVID-19 RNA generating a more potent electric field.

3.4. High-Performance Analysis: Selectivity

The selectivity calculation study involved various In this experiment, approximately 2 µl of 1 µM target sequences were initially used. As shown in Figure 6, at 1 V, the readings. In theory, RNA nucleotides were attached to the AI-IDE through surface amine molecules. Upon hybridization, the charge of RNA from the specimen underwent a sudden alteration. Consequently, the combined charge of the RNA was retained and interacted each other during the measurements. However, introducing various molecules during the immobilization process led to changes in detection sensitivity. While immobilization and hybridization processes with synthetic target probes could generate a robust electrical signal, when the probe interacted with non-complementary and mismatched targets, the current values were nearly identical. This can be attributed to the probe's inability to form a perfect binding with the examined molecules, resulting in similar current responses for non-complementary and mismatched targets.

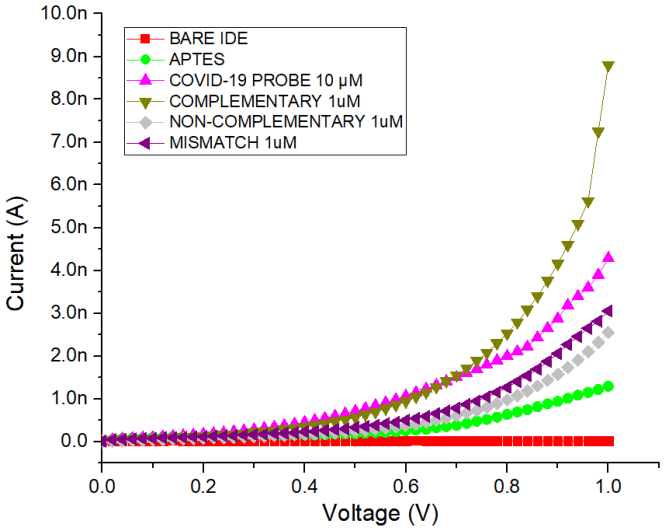

Figure 6. Graph of I-V for Al-IDE with functionalized Al-IDE surface, complementary, non-complementary and mismatched COVID-19 RNA.

3.5. High-Performance Analysis: Sensitivity And Limit of Detection

Sensitivity measurements were conducted by performing I-V characterization with varying concentrations of target COVID-19, as depicted in Figure 7. The current variations consistently increased in correspondence with the increment in target RNA concentration, specifically, resulting in current values at 1 V of 4.95 nA, 5.55 nA, 6.3 nA, and 8.9 nA, respectively. The graph clearly illustrates that the current continues to rise as the concentration of target COVID-19 increases, ranging from low concentrations like fM to higher concentrations up to µM levels. This curve unequivocally indicates that the Al-IDE biosensor is capable of detecting both low and high concentrations of COVID-19 target RNA samples. As the concentration of complementary RNA targets increases, more RNA molecules hybridize with the RNA probe. In conclusion, the Al-IDE biosensor demonstrates clear capability in detecting a wide range of COVID-19 target RNA samples, spanning from low to high concentrations.

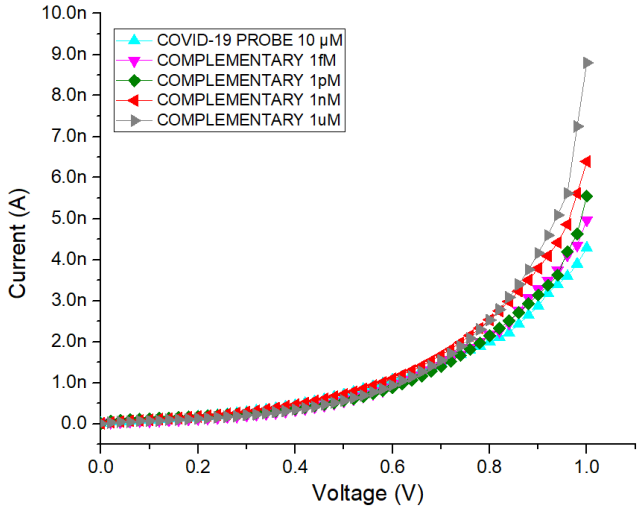

Figure 7. Graph of I-V for Al-IDE with functionalized Al-IDE surface and different concentration target COVID-19 RNA.

4. CONCLUSION

The study introduced an improved method for creating an Al-IDE and assessed its performance in detecting COVID-19. The results demonstrate that this biosensor can effectively detect varying concentrations of complementary RNA sequences associated with COVID-19, showcasing its high sensitivity. Moreover, it exhibits enhanced stability, selectivity, and sensitivity, successfully distinguishing non-complementary and mismatched RNA target sequences. Through the combination of Al-IDE, APTES, and probe RNA, this biosensor development aims to overcome the limitations associated with conventional sensor fabrication, especially in resource-constrained settings. This Al-IDE can detect extremely low concentrations of COVID-19 RNA, making it valuable for both medical and food industry applications due to its ease of production and efficiency. This sensor has the potential to revolutionize the detection not only of COVID-19 but also of newly emerging viruses at the molecular level, offering a solution to address future threats posed by these pathogens.

ACKNOWLEDGMENTS

The author would like to thank all staff members of the Institute of Nanoelectronic Engineering in Universiti Malaysia Perlis (UniMAP) for their technical advice and contributions, directly and indirectly.

REFERENCES

[1] B. A. Taha, Y. Al Mashhadany, M. H. H. Mokhtar, M. S. D. Bin Zan, and N. Arsad, "An analysis review of detection coronavirus disease 2019 (Covid-19) based on biosensor application," *Sensors (Switzerland)*, vol. 20, no. 23, pp. 1–29, 2020, doi: 10.3390/s20236764.

[2] G. Ke *et al.*, "An accurate, high-speed, portable bifunctional electrical detector for COVID-19," *Sci. China Mater.*, vol. 64, no. 3, pp. 739–747, 2021, doi: 10.1007/s40843-020-1577-y.

[3] R. S. Selvarajan, S. C. B. Gopinath, N. M. Zin, and A. A. Hamzah, "Infection-mediated clinical biomarkers for a covid-19 electrical biosensing platform," *Sensors*, vol. 21, no. 11, 2021, doi: 10.3390/s21113829.

[4] N. A. Parmin, U. Hashim, N. Hamidah A Halim, M. N. A. Uda, and M. N. Afnan Uda, "Characterization of Genome Sequence 2019 Novel Coronavirus (2019-nCoV) by using BioinformaticTool," *IOP Conf. Ser. Mater. Sci. Eng.*, vol. 864, no. 1, 2020, doi: 10.1088/1757-899X/864/1/012168.

[5] F. S. Halim *et al.*, "MicroRNA of N-region from SARS-CoV-2: Potential sensing components for biosensor development," *Biotechnol. Appl. Biochem.*, vol. 69, no. 4, pp. 1696–1711, 2022, doi: 10.1002/bab.2239.

[6] A. Tahamtan and A. Ardebili, "Real-time RT-PCR in COVID-19 detection: issues affecting the results," *Expert Rev. Mol. Diagn.*, vol. 20, no. 5, pp. 453–454, 2020, doi: 10.1080/14737159.2020.1757437.

[7] R. D. A. A. Rajapaksha, N. A. N. Yahaya, M. N. A. Uda, and U. Hashim, "Development of portable electronic reader for picoampere detection for two-electrode based amperometric biosensor applications," *AIP Conf. Proc.*, vol. 2045, no. December, pp. 1–7, 2018, doi: 10.1063/1.5080834.

[8] R. D. A. A. Rajapaksha, M. N. A. Uda, U. Hashim, S. C. B. Gopinath, and C. A. N. Fernando, "Impedance based Aluminium Interdigitated Electrode (Al-IDE) biosensor on silicon substrate for salmonella detection," *IEEE Int. Conf. Semicond. Electron. Proceedings, ICSE*, vol. 2018-Augus, pp. 93–96, 2018, doi: 10.1109/SMELEC.2018.8481324.

[9] R. D. A. A. Rajapaksha, U. Hashim, N. Z. Natasha, M. N. A. Uda, V. Thivina, and C. A. N. Fernando, "Gold nano-particle based Al interdigitated electrode electrical biosensor for specific ssDNA target detection," *Proc. 2017 IEEE Reg. Symp. Micro Nanoelectron. RSM 2017*, pp. 191–194, 2017, doi: 10.1109/RSM.2017.8069167.

[10] T. Balasubramaniam *et al.*, "Potential of Syntesized Silica Nanoparticles (Si-NPs) using Corn Cob for Arsenic Heavy Metal Removal," *IOP Conf. Ser. Mater. Sci. Eng.*, vol. 864, no. 1, 2020, doi: 10.1088/1757-899X/864/1/012187.

[11] M. N. A. Uda, S. C. B. Gopinath, U. Hashim, and M. N. A. Uda, "Simple and Green Approach Strategy to Synthesis Graphene Using Rice Simple and Green Approach Strategy to Synthesis Graphene," *IOP Conf. Ser. Mater. Sci. Eng.*, vol. 1, 2020, doi: 10.1088/1757-899X/864/1/012181.

[12] M. N. Afnan Uda, A. B. Jambek, U. Hashim, and M. N. A. Uda, "Electrical DNA Biosensor Using Aluminium Interdigitated Electrode for Salmonella Detection," *IOP Conf. Ser. Mater. Sci. Eng.*, vol. 743, no. 1, 2020, doi: 10.1088/1757-899X/743/1/012022.

[13] M. N. Afnan Uda *et al.*, "Nano-micro-mili Current to Mili Voltage Amplifier for Amperometric Electrical Biosensors," *IOP Conf. Ser. Mater. Sci. Eng.*, vol. 743, no. 1, 2020, doi: 10.1088/1757-899X/743/1/012021.

[14] M. N. Afnan Uda, A. B. Jambek, U. Hashim, M. N. A. Uda, and M. A. F. Bahrin, "Aluminium Interdigitated Electrode Based Biosensor for Specific ssDNA Target Listeria Detection," *IOP Conf. Ser. Mater. Sci. Eng.*, vol. 743, no. 1, 2020, doi: 10.1088/1757-899X/743/1/012032.

[15] R. D. A. A. Rajapaksha, N. A. N. Azman, M. N. A. Uda, U. Hashim, S. C. B. Gopinath, and C. A. N. Fernando, "Multichannel PDMS microfluidic based nano-biolab-on-a-chip for medical diagnostics," *AIP Conf. Proc.*, vol. 2045, no. December, 2018, doi: 10.1063/1.5080833.

[16] M. N. A. Uda, U. Hashim, S. C. B. Gopinath, M. N. A. Uda, N. A. Parmin, and A. M. Isa, "Label-free aptamer based biosensor for heavy metal detection," *AIP Conf. Proc.*, vol. 2291, no. November, 2020, doi: 10.1063/5.0022834.

[17] M. N. A. Uda *et al.*, "Harumanis Mango: Perspectives in Disease Management and Advancement using Interdigitated Electrodes (IDE) Nano-Biosensor," *IOP Conf. Ser. Mater. Sci. Eng.*, vol. 864, no. 1, 2020, doi: 10.1088/1757-899X/864/1/012180.

[18] N. A. N. Yahaya, R. D. A. A. Rajapaksha, M. N. A. Uda, and U. Hashim, "Ultra-low current biosensor output detection using portable electronic reader," *AIP Conf. Proc.*, vol. 1885, 2017, doi: 10.1063/1.5002430.

[19] M. Nur *et al.*, "Conductometric immunosensor for specific Escherichia coli O157 : H7 detection on chemically funcationalizaed interdigitated aptasensor," *Heliyon*, vol. 10, no. 5, p. e26988, 2024, doi: 10.1016/j.heliyon.2024.e26988.

[20] M. N. Afnan Uda, A. B. Jambek, U. Hashim, M. N. A. Uda, and M. A. F. Bahrin, "Development of Internet of Things (IOT) Based Electronic Reader for Medical Diagnostic System," *IOP Conf. Ser. Mater. Sci. Eng.*, vol. 743, no. 1, 2020, doi: 10.1088/1757-899X/743/1/012020.

[21] P. Poltronieri, V. Mezzolla, E. Primiceri, and G. Maruccio, "Biosensors for the Detection of Food Pathogens," *Foods*, vol. 3, no. 3, pp. 511–526, 2014, doi: 10.3390/foods3030511.

[22] M. Xu, R. Wang, and Y. Li, "Electrochemical biosensors for rapid detection of Escherichia coli O157:H7," *Talanta*, vol. 162, no. October 2016, pp. 511–522, 2017, doi: 10.1016/j.talanta.2016.10.050.

[23] M. Mayer and A. J. Baeumner, "A Megatrend Challenging Analytical Chemistry: Biosensor and Chemosensor Concepts Ready for the Internet of Things," *Chem. Rev.*, vol. 119, no. 13, pp. 7996–8027, 2019, doi: 10.1021/acs.chemrev.8b00719.

[24] N. A. Parmin, U. Hashim, S. C. B. Gopinath, and M. N. A. Uda, *Biosensor recognizes the receptor molecules*. Elsevier Inc., 2018.

[25] M. N. A. Uda *et al.*, "Silica and graphene mediate arsenic detection in mature rice grain by a newly patterned current–volt aptasensor," *Sci. Rep.*, vol. 11, no. 1, pp. 1–13, 2021, doi: 10.1038/s41598-021-94145-0.

[26] M. N. A. Uda *et al.*, "Immunosensor development formatting for tungro disease detection using nano-gold antibody particles application," *AIP Conf. Proc.*, vol. 1808, pp. 10–14, 2017, doi: 10.1063/1.4975290.

[27] K. Gherab *et al.*, "Fabrication and characterizations of Al nanoparticles doped ZnO nanostructures-based integrated electrochemical biosensor," *J. Mater. Res. Technol.*, vol. 9, no. 1, pp. 857–867, 2020, doi: 10.1016/j.jmrt.2019.11.025.

[28] M. N. M. N *et al.*, "Top-down nanofabrication and characterization of 20 nm silicon nanowires for biosensing applications," *PLoS One*, vol. 11, no. 3, pp. 20–23, 2016, doi: 10.1371/journal.pone.0152318.

[29] M. A. Fakhri, E. T. Salim, A. W. Abdulwahhab, U. Hashim, and Z. T. Salim, "Optical properties of micro and nano LiNbO3 thin film prepared by spin coating," *Opt. Laser Technol.*, vol. 103, pp. 226–232, 2018, doi: 10.1016/j.optlastec.2018.01.040.

[30] T. B. Tran, S. J. Son, and J. Min, "Nanomaterials in label-free impedimetric biosensor: Current process and future perspectives," *Biochip J.*, vol. 10, no. 4, pp. 318–330, 2016, doi: 10.1007/s13206-016-0408-0.

[31] M. A. Ali, T. A. S. Eldin, G. M. El Moghazy, I. M. Tork, and I. I. Omara, "Original Research Article Detection of E . coli O157 : H7 in feed samples using gold nanoparticles sensor," *Int. J. Curr. Microbiol. Appl. Sci.*, vol. 3, no. 6, pp. 697–708, 2014.

[32] V. K. Nigam and P. Shukla, "Enzyme based biosensors for detection of environmental pollutants-A review," *J. Microbiol. Biotechnol.*, vol. 25, no. 11, pp. 1773–1781, 2015, doi: 10.4014/jmb.1504.04010.

[33] Y. Wu and H. Chai, "Development of an electrochemical biosensor for rapid detection of foodborne pathogenic bacteria," *Int. J. Electrochem. Sci.*, vol. 12, no. 5, pp. 4291–4300, 2017, doi: 10.20964/2017.05.09.

[34] C. Song, J. Li, J. Liu, and Q. Liu, "Simple sensitive rapid detection of Escherichia coli O157:H7 in food samples by label-free immunofluorescence strip sensor," *Talanta*, vol. 156–157, pp. 42–47, 2016, doi: 10.1016/j.talanta.2016.04.054.

[35] Y. Song, Y. Luo, C. Zhu, H. Li, D. Du, and Y. Lin, "Recent advances in electrochemical biosensors based on graphene two-dimensional nanomaterials," *Biosens. Bioelectron.*, vol. 76, pp. 195–212, 2016, doi: 10.1016/j.bios.2015.07.002.